Electronic Supplementary Material (ESI) for Physical Chemistry Chemical Physics

Supplementary Information

Hydrogen and Carbon Monoxide Generation from Laser-Induced Graphitized Nanodiamonds in Water

Dong Myung Jang, Hyung Soon Im, Yoon Myung, Yong Jae Cho, Han Sung Kim, Seung Hyuk Back, Jeunghee Park, Eun Hee Cha, and Minyung Lee

Figure S1. (a) Photograph of aqueous ND solution (80 mg/L) before (0 h) and after 1 h, 2 h, 3 h, and 4 h of 532 nm (80 mJ/pulse) laser irradiation shows that a light brown color becomes to a dark brown one due to the surface graphitization. Their UV-visible absorption spectrum indicates that laser irradiation increases the absorption in the visible range (>400 nm), while decreases it in the UV range. (b) Photograph and UV-visible absorption spectrum of aqueous 0.2 mM $HAuCl_4$ solution containing ND (80 mg/L) before (0 h) and after 30 min, 1 h, 2 h, and 4 h of laser irradiation. The Au-ND solution shows a faster darkening (graphitization) than the ND solution; the time required for full darkening is 3 h (ND) and 1 h (Au-ND).

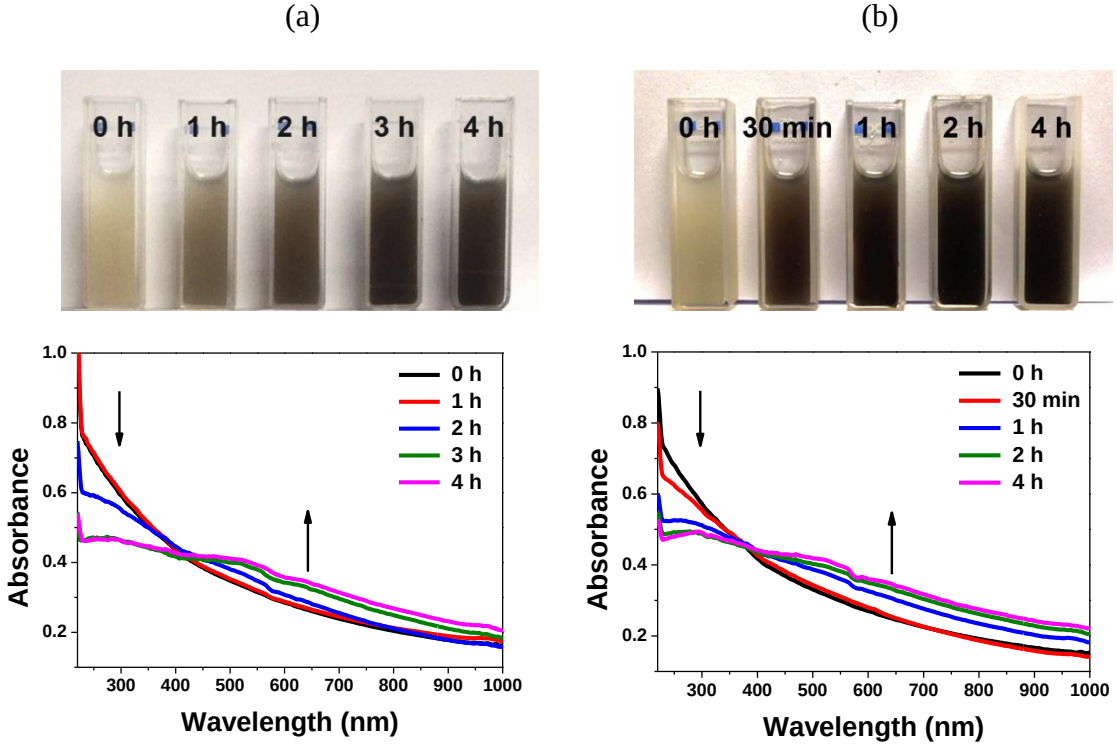

Figure S2. Cyclic voltammetry (CV) curves (vs. Ag/AgCl reference electrode) of the ND (hydrogen treated ND which was used in the present experiment) (a) before and (b) after the 4 h laser irradiation was measured using 10 and 50 mV/s scan rate.

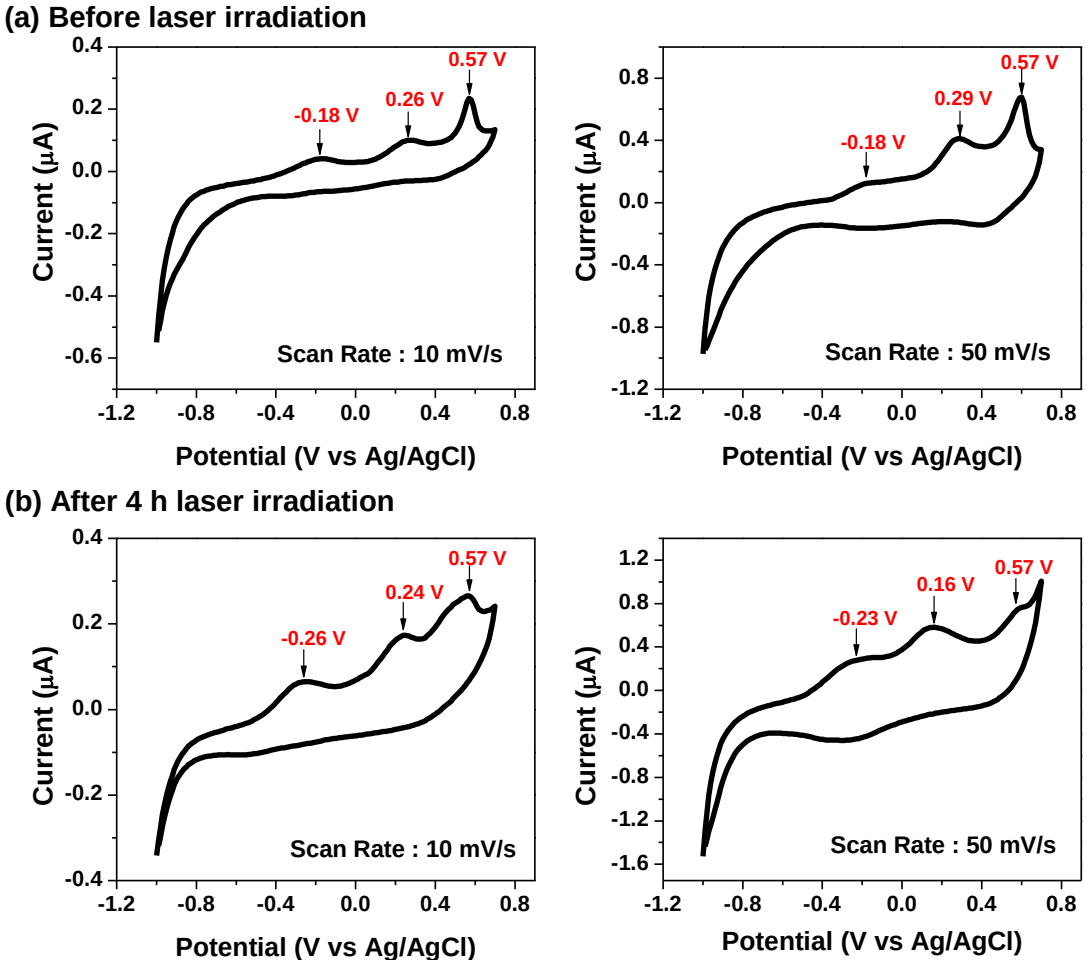

The CV curves were recorded on an IVIUM CompactStat electrochemical analyzer using gold (area ca. 0.02 cm^2) disks as the working electrode, a Pt-wire auxiliary electrode and Ag/0.01 M $AgNO_3$ reference electrode (BAS Inc., 0.1 M tetrabutylammonium hexafluorophosphate ($TBAPF_6$)/acetonitrile electrolyte). A drop of the 1 mg of ND dispersed in 1 mL of isopropyl alcohol solution was placed on the polished surface of the working electrode and then the solvent was evaporated to form a film. The electrolytes were

thoroughly deoxygenated by bubbling with high-purity argon for 15 min. The VB band energy were calculated from the E_{ox} value, assuming the energy level of ferrocene/ferrocenium (Fc/Fc^+) to be -4.8 eV below the vacuum level. The formal potential of Fc/Fc^+ was measured to be 0.095 V against an Ag/Ag^+ reference electrode. Therefore, E_{VB} (E_{HOMO}) = -(E_{ox} +4.705) eV, where the onset potential values were relative to the Ag/Ag^+ reference electrode.

We could not obtain the CV curved from the purified and oxygen treated ND due to their lower conductivity. The ND (before irradiation) shows three oxidation peaks at -0.18, 0.26, and 0.57 V (scan rate = 10 mV/s). From the lowest potential peak (-0.18 V), the position of VB was estimated to be E_{VB} = -4.525 eV. The other two peaks became more prominent in the repetitive scans, indicating a change in surface states involving the oxide groups. The ND (after irradiation) also shows the lowest oxidation peaks at -0.26 V (scan rate = 10 mV/s), suggesting E_{VB} = -4.475 eV, which was close to that (work function) of graphene; -4.57 eV [Reference: Y. -J. Yu, Y. Zhao, S. Ryu, L. E. Brus, K. S. Kim, and P. Kim, *Nano Lett.*, 2009, **9**, 3430].

Figure S3. Time-dependent H_2, CO, and CH_4 evolution (μmol) from the (a) reduced graphene oxide (RGO) and (b) multi-walled carbon nanotubes (MWCNT, Sigma-Aldrich Co., outer diameter = 20~40 nm, inner diameter = 5~10 nm, length = 0.5~50 μm) solution (20 mg/100 mL) under laser irradiation (80 mJ/pulse). Graphene oxide was synthesized from graphite by Hummers' exfoliation method [Hummers, W. S. Jr.; Offeman, R. E. *J. Am. Chem. Soc.* **1958**, *80*, 1339], and was reduced into RGO using heating in H_2 flow at 800 °C for 1 h. For RGO, the avg. evolution rate of H_2, CO, and CH_4 is 115, 231, and 3 μmol/mol, respectively. MWCNT show the avg. evolution rate of H_2, CO, and CH_4 as 70, 142, and 3 μmol/mol, respectively. The ratio of $[H_2]/[CO]$ is about 0.5. The evolution rate follows the order RGO > MWCNT > ND.

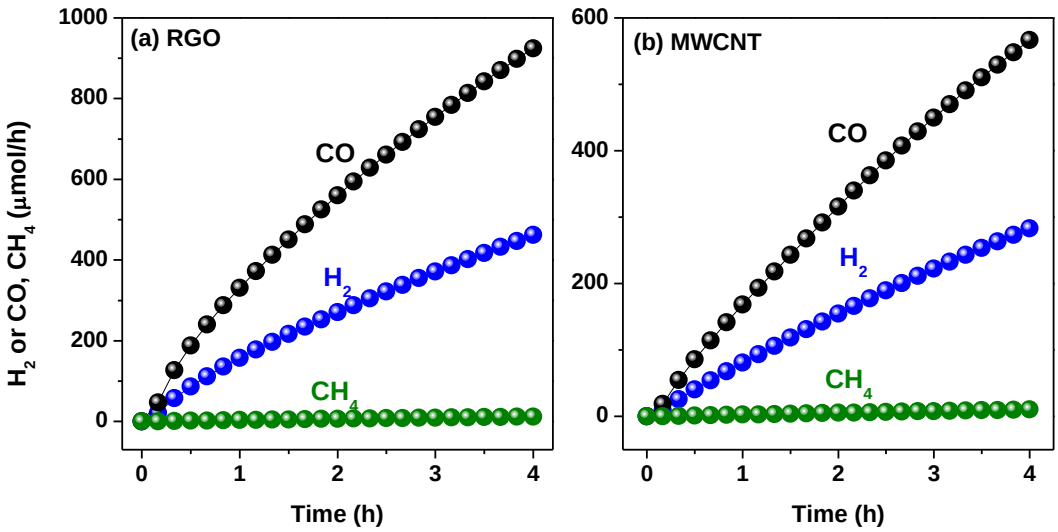

Figure S4. IR spectra of the ND before and after 4 h laser irradiation, and metal-ND hybrid nanostructures (after 4 h laser irradiation). The peak at 3420 cm^{-1} is assigned to the O-H stretching vibration modes in alcoholic or carboxylic groups. The peaks at 2960, 2925, and 2855 cm^{-1} are assigned to the C-H stretching vibration modes. Both ND and NP-ND exhibited common enhancement in the peaks related with the C-H bonds, resulting in the nearly similar IR spectrum after the laser irradiation.

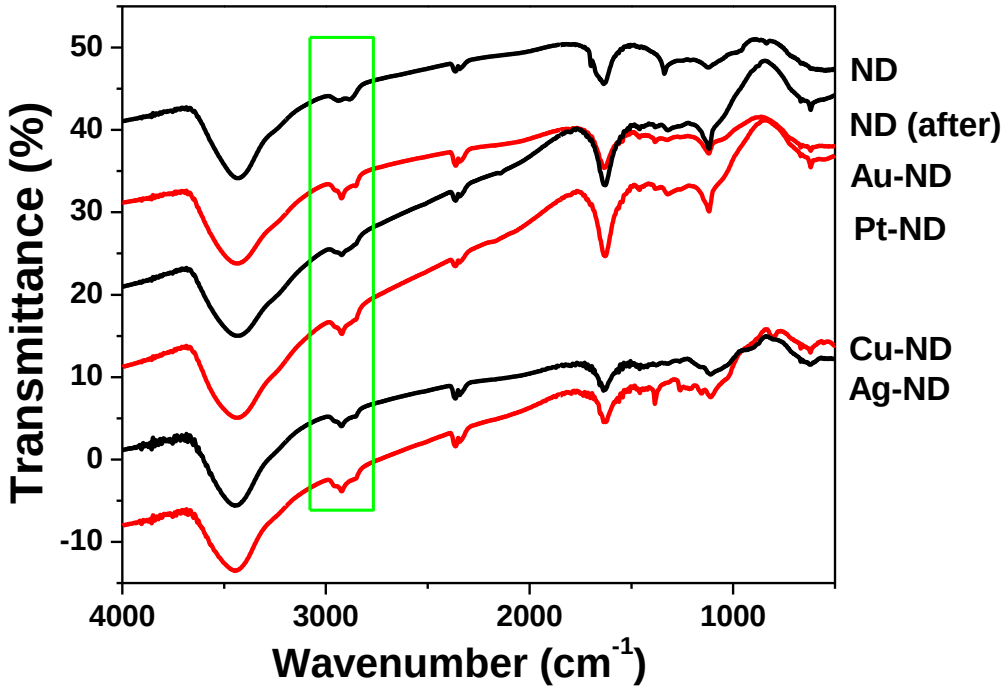

Figure S5. (a) Photograph of aqueous Au, Ag, and Pt precursor solutions containing ND, before and after laser irradiation. TEM images identify the production of the metal NP. (b) UV-visible spectrum of the Au, Ag, and Pt NP in water. The aqueous metal precursor solutions (0.2 mM, 10 mL) were prepared and mixed with 1 mg of ND accordingly, and illuminated by laser pulses. The photograph demonstrates the change in color of the solutions due to the production of respective metal NP. The synthesis of colloidal Au, Pt, and Ag NP was completed after about 30, 60, and 60 min irradiation, respectively, which was confirmed by their TEM images and UV-visible absorption spectrum. The Au and Ag NPs show a typical surface plasmon (SP) band at 540 and 410 nm, respectively. The "without ND" solution shows no color change.

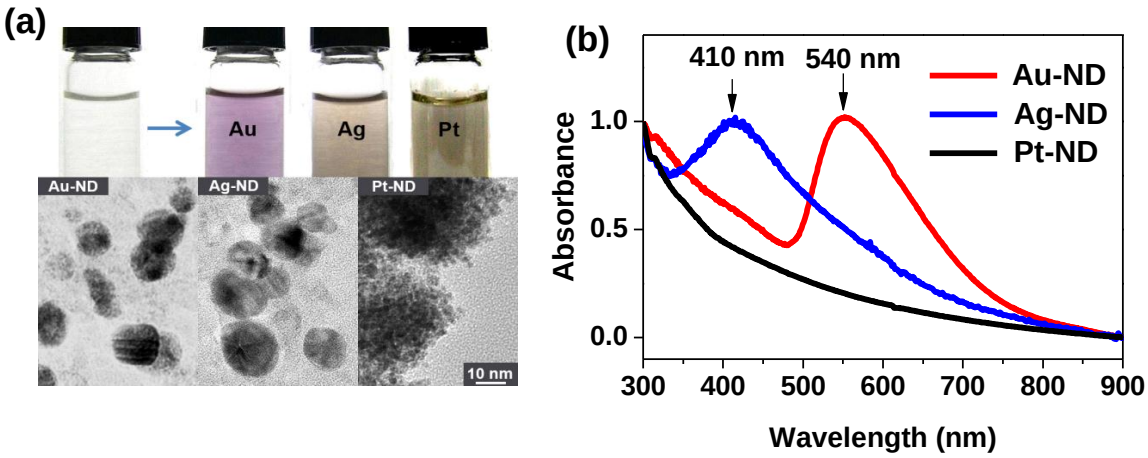

Figure S6. A plot of summed H_2 and CO generation rate versus the standard reduction potential of metal ions (versus H^+/H_2); 1.69 eV (Au^+), 1.2 eV (Pt^{2+}), 0.99 V (Pd^{2+}), 0.79 eV (Ag^+), and 0.53 eV (Cu^+).

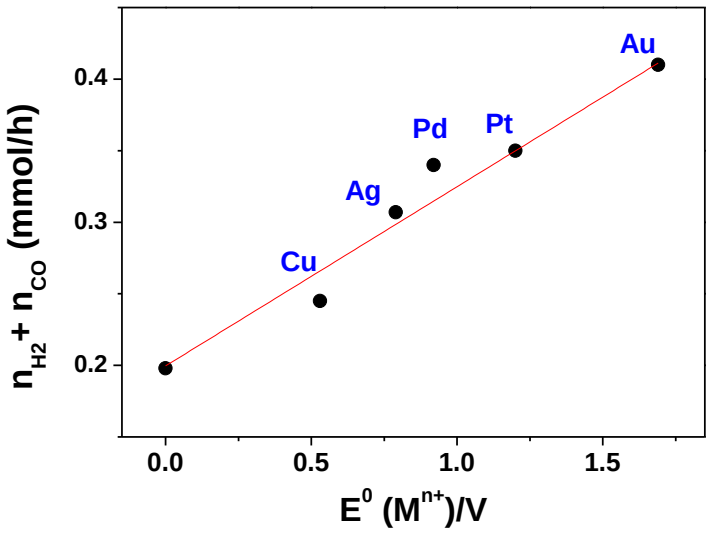

Figure S7. HRTEM images of the (a) Pt-ND and (b) Ag-ND hybrid nanostructures, after 4h 532 nm laser irradiation. The distances between the adjacent (111) planes of the Pt and Ag were 2.3 and 2.4 Å, which are close to those of cubic Pt (04-0802; a = 3.890 Å) and Ag (87-0720; a = 4.077 Å), respectively. (c) The EDX data confirming the composition of metal NP-ND hybrid nanostructures.

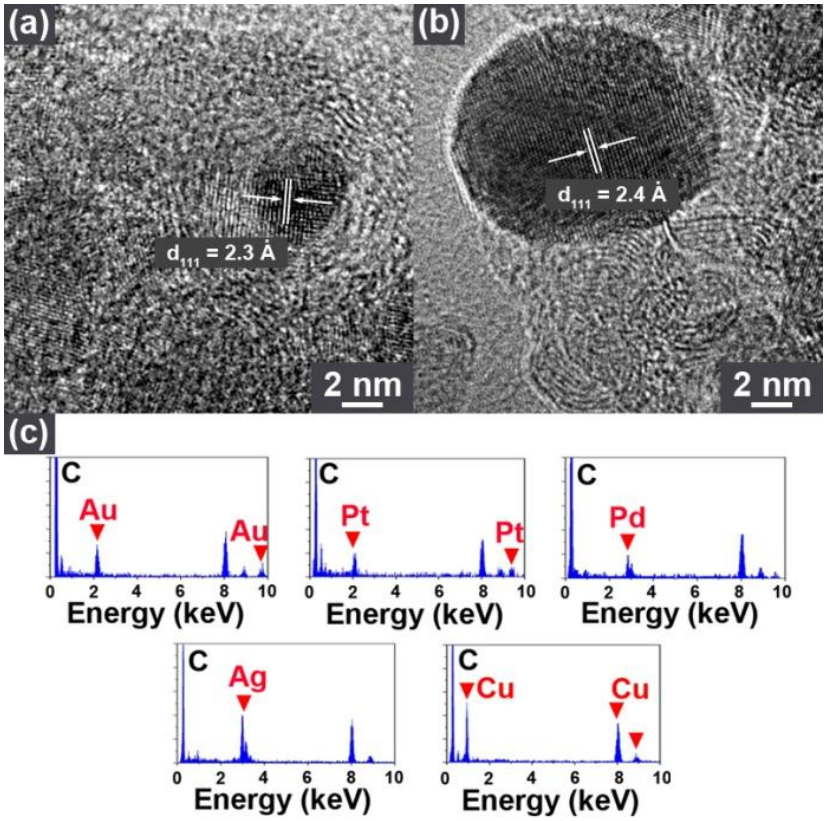

Figure S8. XPS of Au-ND, Pt-ND, Pd-ND, Ag-ND, and Cu-ND, showing avg. 0.5 at. % of metal NPs; 0.4 % Au, 0.4 % Pt, 0.7 % Pd, 0.6 % Ag, and 0.4 % Cu.

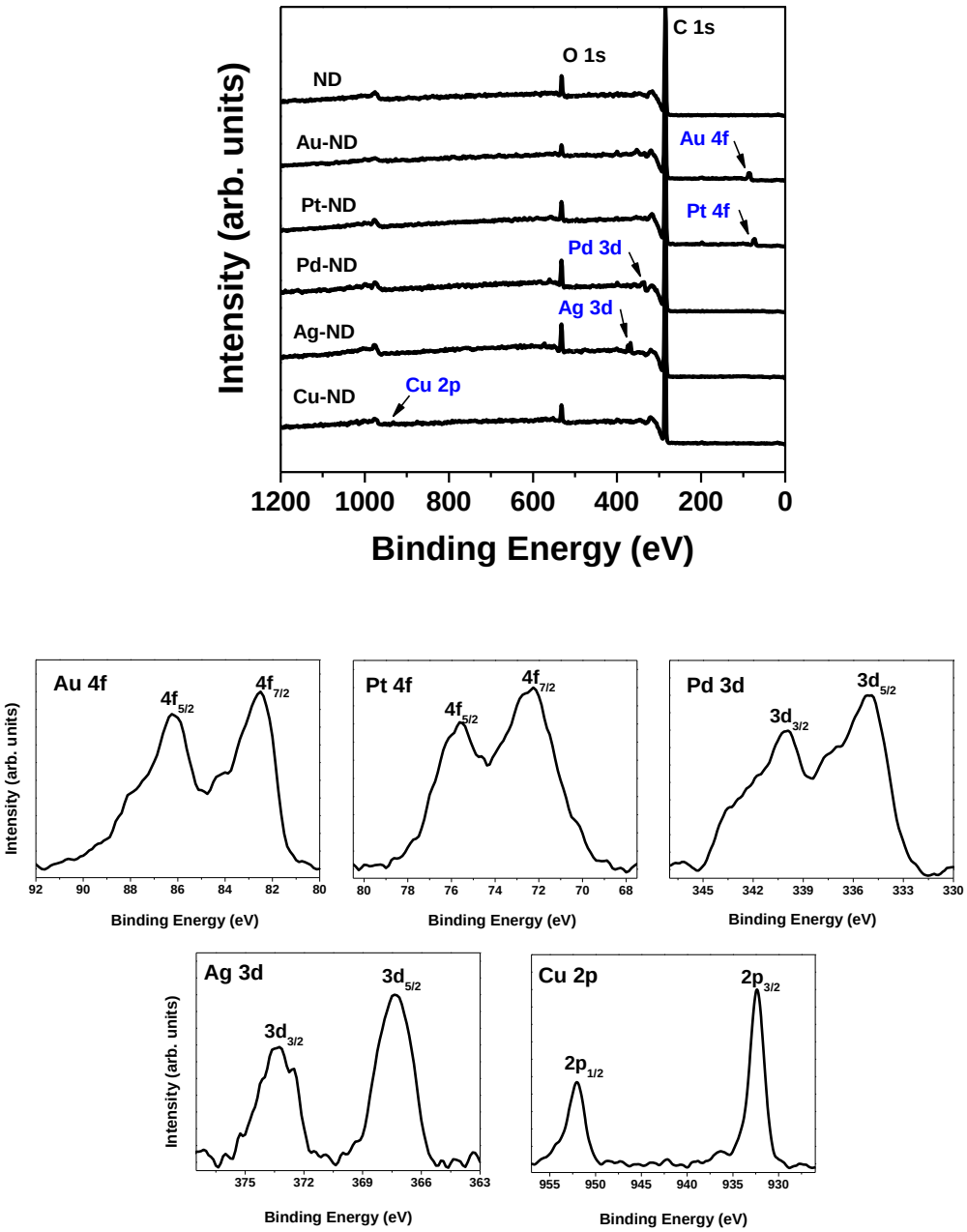

Figure S9. XRD patterns of ND, Au-ND, Pt-ND, Pd-ND, Ag-ND, and Cu-ND, confirming high purity of cubic phase metal NPs. The peaks were in match with the diamond (JCPDS No. 75-0624; a = 3.566 Å), Au (JCPDS No. 04-0784; a = 4.078Å), Pt (JCPDS No. 04-0802; a = 3.890 Å), Pd (JCPDS No. 87-0645; a = 3.867 Å), Ag (JCPDS No. 87-0720; a = 4.077 Å), and Cu (JCPDS No. 85-1326; a = 3.615 Å).

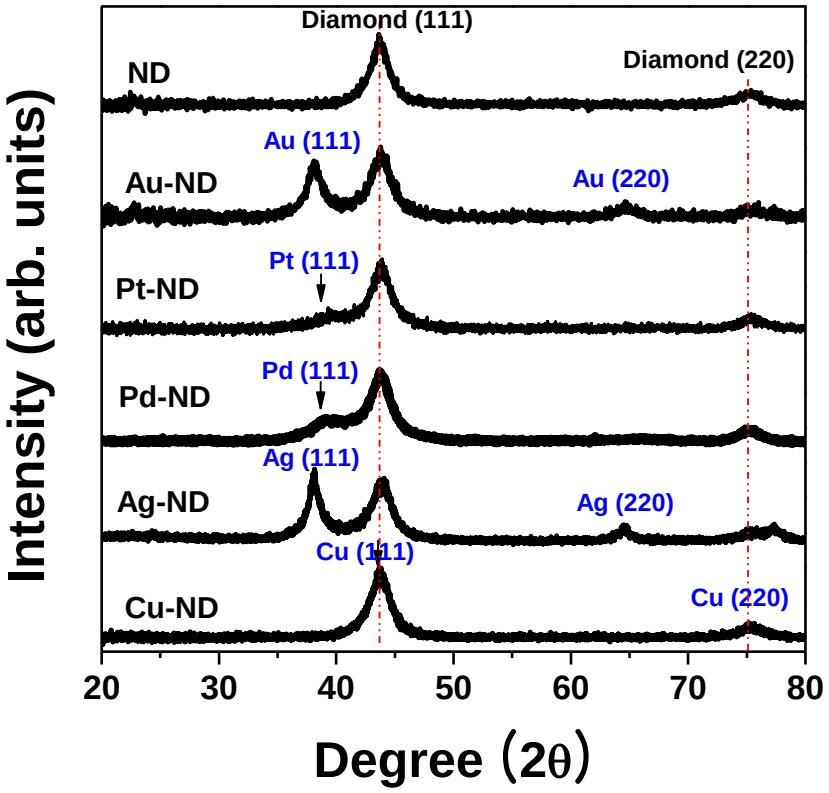

Figure S10. (a) HRTEM images of the Au-RGO (size of Au nanocrystals = 3 nm) and (b) I–V characteristics using a 514 nm Ar ion laser irradiation (10 mW) and in the dark, and their respective ΔI–t curves under chopped irradiation (inset).

For the synthesis of Au-RGO hybrid nanostructures, 6×10^{-3} mmol (2.4 mg) hydrogen tetrachloroaurate trihydrate ($HAuCl_4\cdot3H_2O$) were dissolved in 15 mL oleylamine (OLA) containing 24 mg of RGO. The mixture was vigorously stirred for 1 h. 7.2×10^{-3} mmol (0.22 mg) ammonia borane (NH_3BH_3) dissolved in OLA was quickly added to the Au solution. The mixture was stirred for 30 s. Ethanol was added to precipitate the products, which were washed with ethanol and isolated by centrifugation.